

Evidence of Carrier Localization in AlGa_N/Ga_N-Based UV Multiple Quantum Wells with Opposite Polarity Domains Provided by Nanoscale Imaging

Mei Cui, Wei Guo,* Houqiang Xu, Jie'an Jiang, Li Chen, Somak Mitra, Iman S. Roqan, Haibo Jiang, Xiaohang Li, and Jichun Ye*

AlGa_N-based multiple quantum wells (MQWs) incorporating opposite polarity domains are grown by metal–organic chemical vapor deposition (MOCVD). A direct demonstration of the carrier localization effect is provided by a combination analysis of space-resolved luminescence peak position and Ga/Al composition distribution. Furthermore, through Raman spectroscopy, it is found that compressive strain plays a key role in improving the optical properties of UV-MQWs despite the inferior crystalline quality in the N-polar domains. This suggests that incorporating sub-micrometer-scale polarity domains in the MQWs is promising for the development of efficient UV emitters.

1. Introduction

UV light-emitting diodes (UV-LEDs) have drawn tremendous attention in the past decade due to their wide applications in resin curing, water/air purification, and biochemical sensing.^[1–6] However, the external quantum efficiencies (EQEs) of UV-LEDs

are generally far lower than those of the InGa_N-based visible LEDs^[7,8] due to high-density defects, difficulties in p-type doping, and larger polarization field in AlGa_N thin film. This requires an in-depth exploration on the optimized design of the active region in the UV-LEDs and deeper understanding on the carrier recombination processes.

Because of the noncentrosymmetric crystallographic orientation of III-nitrides, III- and N-polarity surfaces can be achieved along the *c*-axis. Conventionally, III-polarity is more commonly used in device fabrication due to smooth surface morphology

and high crystalline quality.^[9] N-polar surface, on the other hand, has many other advantages such as increased carrier injection efficiency^[10] and reduced quantum-confined Stark effect (QCSE) under forward bias condition.^[11] But, progress in growing N-polar epitaxial thin films is still lagging behind due to high densities of threading dislocations (TDs) and point defects, which strongly deteriorates device performance.^[12] This necessitates the search for novel optoelectronic devices taking advantages of both III- and N-polar domains.

It has been previously reported by Mita and Hite that the polarities of III-nitride epitaxial thin films can be controlled by low-temperature (LT) AlN nucleation layers (NLs).^[13] A macroscale lateral polarity structure (LPS) was fabricated by substrate patterning followed by epitaxial growth through metal–organic chemical vapor deposition (MOCVD) with III- and N-polarity domains simultaneously grown side-by-side.^[14] Utilizing this structure, Collazo et al. reported a depletion-mode metal–semiconductor field-effect transistor (MESFET) on LPS-GaN with improvement in contact resistance.^[15] Sheikhi et al. reported the usage of LPS-GaN in the fabrication of Schottky barrier diode (SBD) with smaller on-state resistance and larger rectification ratio.^[16] Optical property of the LPS, on the other hand, has seldom been investigated in the past decades. Kirste et al. fabricated an LPS-based GaN thin film and observed a strong photoluminescence (PL) intensity at the domain boundary.^[17] It is noted that, once LPS is introduced into heterostructures such as UV-LEDs, various interfaces will inevitably add to the complexity of the carrier distributions and recombination processes. A few works have been carried out so far.^[14,16–18] A recent study of our group demonstrated that by scaling down the size of both III- and N-polar domains to only several micrometers, and incorporating LPS into AlGa_N/Ga_N multiple quantum wells (MQWs),

M. Cui, Prof. W. Guo, H. Xu, J. Jiang, Dr. L. Chen, Prof. J. Ye
Ningbo Institute of Materials Technology and Engineering
Chinese Academy of Sciences
Ningbo, Zhejiang 315201, China
E-mail: guowei@nimte.ac.cn; jichun.ye@nimte.ac.cn


M. Cui, Prof. W. Guo, H. Xu, J. Jiang, Dr. L. Chen, Prof. J. Ye
University of Chinese Academy of Sciences
Beijing 100049, China

J. Jiang
School of Physical Science and Technology
ShanghaiTech University
Pudong, Shanghai 201210, China

Dr. S. Mitra, Prof. I. S. Roqan
Physical Science and Engineering Division
King Abdullah University of Science and Technology (KAUST)
Thuwal 23955, Saudi Arabia

Prof. H. Jiang
School of Molecular Sciences
University of Western Australia
Perth 6009, Australia

Prof. X. Li
Advanced Semiconductor Laboratory
King Abdullah University of Science and Technology (KAUST)
Thuwal 23955, Saudi Arabia

 The ORCID identification number(s) for the author(s) of this article can be found under <https://doi.org/10.1002/pssr.202100035>.

DOI: 10.1002/pssr.202100035

dramatically different optical behaviors were identified.^[19] Higher luminescence intensity was observed in N-polar than in III-polar domains, which can be ascribed to thickness fluctuations in N-polar domains as previously demonstrated by transmission electron microscopy (TEM).^[20,21] However, it must be noted that in addition to that, composition fluctuation and strain variation also play critical roles in the carrier localization effect, which has never been investigated before and, thus, requires in-depth investigations, especially from the perspective of nanoscale mapping.

In this work, a direct demonstration of the carrier localization effect is provided by a combined analysis of spatially resolved PL mapping, composition distribution, and Raman spectroscopy. The contribution from each factor is thoroughly discussed, and the overall influence on the carrier localization effect is revealed.

2. Experimental Section

The epitaxial growth of UV-MQWs starts with the patterning of LT AlN-NL. **Figure 1a** schematically shows the fabrication

process of an LPS with AlGaIn/GaN MQWs and corresponding thickness/composition information. A 20 nm thick AlN-NL was first grown on a 2 in. sapphire substrate. The NL patterning was achieved using a nanosphere lithography technique through polystyrene (PS) sphere coating followed by reactive ion etching (RIE).^[22] Self-assembled PS spheres on top of the AlN-NL were formed via a large-area micropropulsive injection (MPI) method. Details on the preparation techniques were described elsewhere.^[23] The PS sphere diameters were then reduced by O₂ plasma trimming. The exposed LT-NLs in the gaps between PS spheres were etched by plasma etching using a mixture of Cl₂ and BCl₃ plasma with the flow rates of 10 and 25 sccm, respectively, whereas the AlN-NLs beneath PS spheres remained intact. The bias and inductively coupled plasma (ICP) powers are 100 and 300 W during the process. The periodicity of AlN-NL patterning is 6 μm, with spacing between each pattern being 1.5 μm after etching. Patterned substrates were then reloaded into the MOCVD chamber for epitaxial regrowth. Trimethylaluminum (TMA), triethylgallium (TEG), and ammonia (NH₃) were used

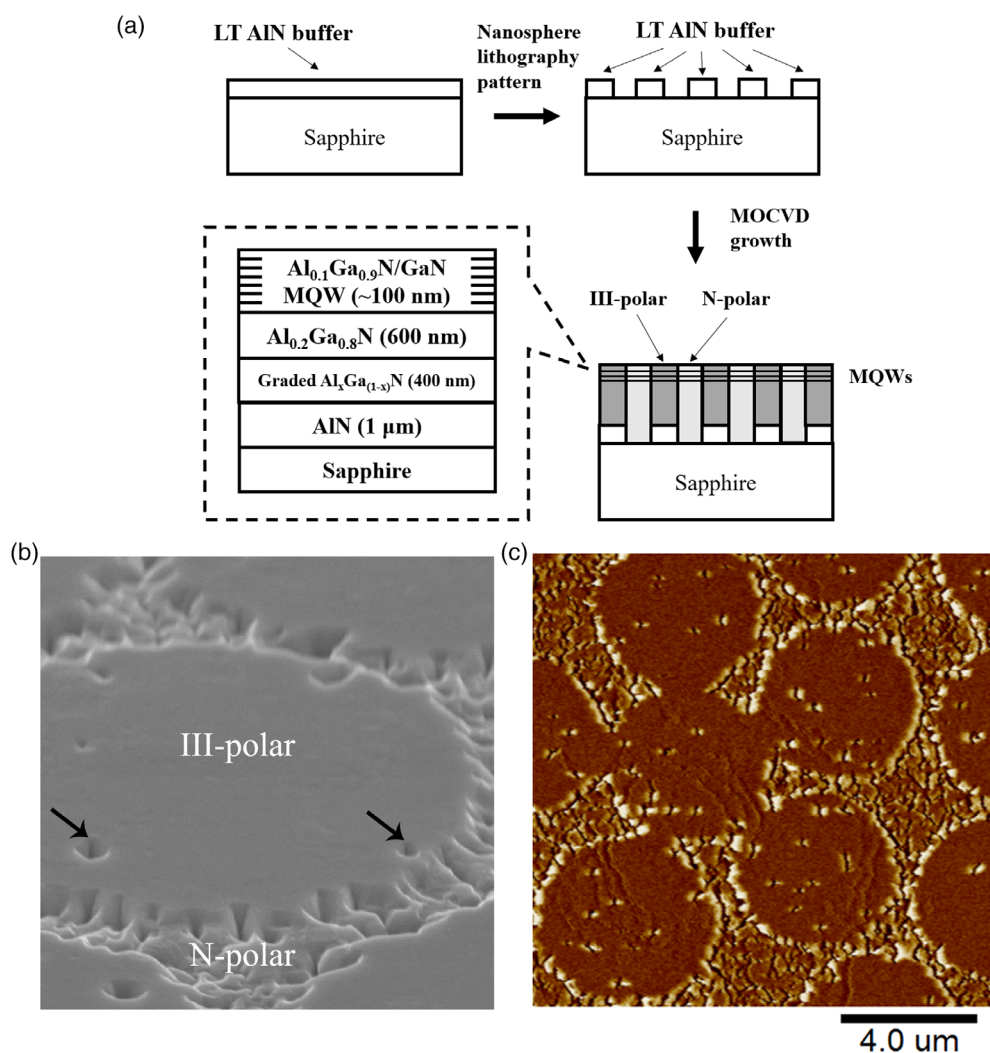


Figure 1. a) Schematic illustration on the fabrication process of LPSs and corresponding structural information. b) 30° tilted view SEM images of the as-grown LPS MQWs. Smooth III-polar domains and rough N-polar domains are notified. Pit-like features inside III-polar domains are indicated by the black arrows. c) Corresponding PFM phase signals of the LPS for polarity identification.

as precursors of Al, Ga, and N, respectively. The whole epitaxial structure of the MQW consists of 1 μm AlN thin film, 400 nm thick $\text{Al}_x\text{Ga}_{1-x}\text{N}$ template with composition grading from $x = 0.6$ to $x = 0.3$, 600 nm thick $\text{Al}_{0.2}\text{Ga}_{0.8}\text{N}$ template, and ten pairs of $\text{Al}_{0.1}\text{Ga}_{0.9}\text{N}/\text{GaN}$ MQWs; 1 μm AlN template and epitaxial layers on top were grown at the temperatures of 1250 and 1100 $^{\circ}\text{C}$, respectively. For comparison purpose, uniform III- and N-polar MQWs were grown on uniform AlN-NL and bare sapphire substrates, respectively, under the same growth condition.

Surface morphologies of the samples were characterized using a Hitachi S-4800 field-emission scanning electron microscope (SEM) and a Veeco Dimension 3100 V atomic force microscope. Polarity identification was performed using the same atomic force microscopy tool mentioned earlier, but operated under a scanned-probe mode based on the converse piezoelectric effect, i.e., piezoresponse force microscopy (PFM).^[24] Steady-state PL characterization and time-resolved PL (TRPL) experiments were performed with a mode-locked Ti:sapphire laser at 5 K. A third harmonic generator (APE-SHG/THG) was used to excite the samples by an output wavelength of 266 nm (pulse width of 150 fs and pulse repetition rate of 76 MHz). Spatially resolved PL mapping was performed using a Renishaw inVia Reflex spectrometer system equipped with a 325 nm laser. Thin-film composition and crystalline quality were characterized using a Bruker D8 DISCOVER high-resolution X-ray diffraction (HRXRD) instrument. Relative atomic compositions were studied by the nanoscale secondary ion mass spectroscopy (nano-SIMS) using a Cameca NanoSIMS 50L system. Strain analysis and local thin-film quality were carried out using the same equipment as that of PL mapping, but with a 532 nm neodymium: yttrium aluminum garnet (Nd:YAG) laser as the excitation source.

3. Results and Discussion

Figure 1b shows the tilted view scanning electron microscopy (SEM) images of the LPS sample. Circular-shaped III-polar domains and surrounding N-polar domains exhibit dramatically different surface morphologies due to variations in surface

energies and consequently different growth modes.^[25] The III-polar domains are slightly taller than adjacent N-polar domains. Several pit-like features within smooth III-polar domains are marked by black arrows, which could possibly be due to either the existence of nanoscale inversion domains (IDs) or simply the formation of V-defect due to lattice and thermal mismatch.

The polarities of III-nitrides were identified by PFM, as shown in Figure 1c. As III- and N-polar domains have opposite spontaneous polarization fields, therefore, PFM images are able to reveal different polarity domains through phase signal.^[24] In-phase matching between the applied tip bias and the measured deflection signal is typically observed in N-polar domains, whereas the bias and deflection signals are out-of-phase for III-polar domains.^[24] As clearly observed in Figure 1c, III-polar domains are represented by out-of-phase signals with negative values, whereas N-polar domains are evidenced by the positive in-phase values. The colors near the interface between the III- and N-polar domains are relatively brighter, indicating a higher polarization field and stronger carrier accumulations there, consistent with previous reports by Kirste et al.^[17]

To understand the optical behaviors of the MQWs with opposite polarity domains, steady-state PL spectra were first collected on uniform III-polar, N-polar, and LPS MQWs, respectively, at 5 K. Pumping power was kept as 50 mW cm^{-2} . As shown in Figure 2a, the LPS sample exhibits the strongest PL intensity, demonstrating its high radiative recombination efficiency compared with uniform polar samples. Furthermore, the luminescence intensity of uniform N-polar sample is higher than that of the III-polar sample. This could originate from the rough surface morphology, and consequently, a strong carrier localization effect was induced by the composition and thickness nonuniformity in N-polar sample. The strong PL intensity in the N-polar surface is consistent with the cathodoluminescence (CL) mapping shown in our previous work, where quantum-dot-like luminescence centers were observed.^[20] Peak positions for uniform III-polar, N-polar, and LPS MQWs are 355, 360, and 350 nm, respectively. More than 10 nm peak shift is observed among all samples. As all the samples were grown in MOCVD chamber at the same time, the discrepancy of peak emission wavelengths can be ascribed to different carrier confinement properties

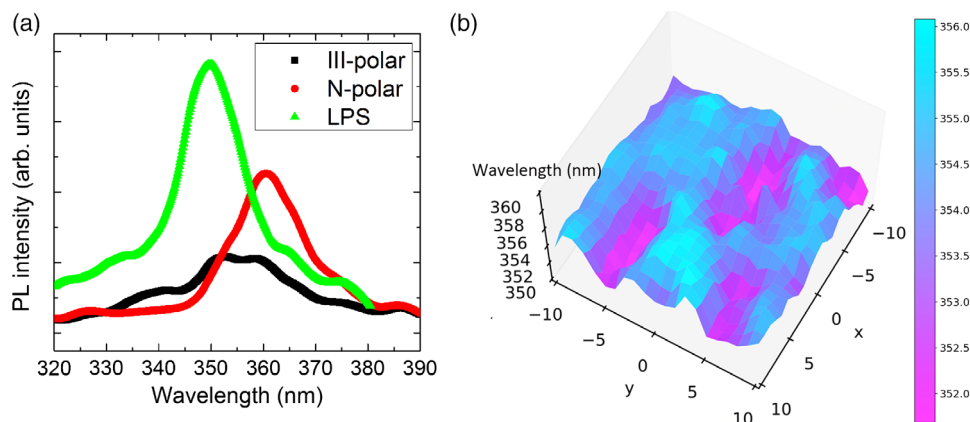


Figure 2. a) PL spectra of uniform III-polar, N-polar, and LPS MQWs collected at 5 K. b) 3D color map of the emission wavelength distribution within the LPS MQW sample.

within different polarity domains of the MQW region.^[26] Inside the LPS-based MQW, the distribution of PL peak position was further analyzed by spatially resolved PL mapping. The 3D mapping of peak position in a $20 \times 20 \mu\text{m}^2$ region is shown in Figure 2b. Interestingly, a negligible 4 nm peak variation was obtained between III- and N-polar domains within the LPS sample, and there is no correlation between the peak maximum or minimum and the locations of the polarity domains. This strongly suggests that the 10 nm blueshift in the LPS from Figure 2a is not solely dependent on thin-film polarity.

Note from Figure 2a that the uniform III-polar MQW exhibits the lowest PL intensity. To investigate the influence of crystalline quality on the optical behaviors, XRD rocking curves (RCs) on (002) diffraction peaks of MQW region were characterized and are shown in Figure 3a. The full-width-half-maximum (FWHM) of the diffraction peaks is 0.334° , 0.435° , and 0.317° for uniform III-polar, uniform N-polar, and LPS samples, respectively. The TD densities are calculated to be $3.1 \times 10^9 \text{ cm}^{-2}$, $5.3 \times 10^9 \text{ cm}^{-2}$, and $2.8 \times 10^9 \text{ cm}^{-2}$. Referring the low PL intensity of the uniform III-polar sample, it is concluded that optical property has weak dependence on crystalline quality. In fact, the relatively higher PL intensity in N-polar and LPS samples can be

explained by the composition and thickness nonuniformity in the MQWs. This leads to a carrier localization effect and much stronger radiative recombination rate in the active region, which has been reported in our previous work.^[27] Figure 3b shows the ω - 2θ scans of all samples. The MQW diffraction peaks with $N=0$ are located at $2\theta = 34.59^\circ$, 34.60° , and 34.65° for uniform III-polar, N-polar, and LPS samples. Therefore, the average Al compositions in the MQW active regions are 1.6%, 2.3%, and 5.8%. Note that these are average values considering the composition and thickness of both $\text{Al}_{0.1}\text{Ga}_{0.9}\text{N}$ quantum barrier (QB) and GaN QW. The variation is possibly due to different adatom incorporation rates in III- and N-polar surfaces and influence from rough surface morphology. Also notice that the XRD peak position of $\text{Al}_{0.2}\text{Ga}_{0.8}\text{N}$ template follows the same trend, suggesting that composition variation already started during the AlGaN template growth. Nevertheless, if the PL emission is solely dependent on Al composition, then a maximum 7.7 nm peak shift is obtained (361.8, 360.5, and 354.1 nm for abovementioned three samples derived from the average MQW composition). This result is obviously against the large variation of PL wavelengths, as shown in Figure 2a. Therefore, the investigation of optical behaviors of these samples should consider not only thin-film composition, but also carrier localization effect as mentioned before.

To further understand the carrier dynamic properties of the UV-MQW samples, time-resolved and wavelength-dependent TRPL study of uniform III-polar, N-polar, and the LPS samples are compared in Figure 4a. The x-axis denotes the wavelength, and the y-axis is the relative time. The decay profiles of all the samples depend on the wavelength. For uniform III-polar sample, two dominant emission peaks are observed at 340 and 350 nm, respectively. The 350 nm peak shows a much stronger intensity and also relatively slower decay curve. For uniform N-polar sample, three peaks can be identified, locating at 352, 355, and 358 nm, respectively. These three peaks might be correlated with different energy states in the MQWs due to thickness fluctuations in the N-polar MQW region.^[20] In comparison with uniform III- and N-polar MQWs, LPS-MQW shows a rather uniform decay profile. Only one single peak at 347 nm was identified. At peak wavelengths, the TRPL intensity of LPS MQW and uniform polar MQWs all follow a monoexponential decay, as shown in Figure 4b, suggesting the negligible influence from nonradiative recombination at LT. After calculation, the decay lifetimes of uniform III-polar, N-polar MQWs, and LPS MQW are 1.79, 1.96, and 0.56 ns, respectively. The shortest decay lifetime of LPS-MQW suggests a much faster recombination channel and, consequently, higher radiative recombination rate.^[28,29]

As identified earlier, there is a wavelength variation among the PL spectra of uniform III-, N-polar, and LPS-based MQWs. Control of the emission wavelength is challenging, because it is related to various factors, including alloy compositions, QW confinement, and strain conditions of the active regions.^[30,31] Introduction of different polarity domains into the system makes it even more complex. Thus, it is crucial to distinguish the contribution of each factor. Herein, nano-SIMS characterization of the LPS was performed with a collection depth near the surface where the MQWs are located. Figure 5a highlights the different element concentrations between III- and N-polar domains of the LPS samples with $6 \mu\text{m}$ periodicity. Line scans from two

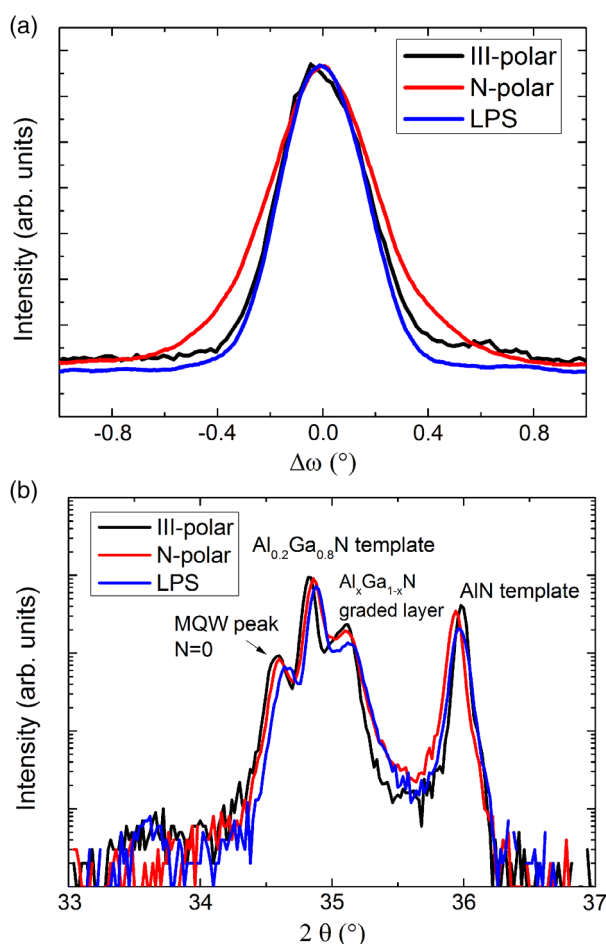


Figure 3. a) Symmetric (002) XRD RC scans of the MQWs from uniform III-polar, N-polar, and LPS samples. b) ω - 2θ scans of these three samples for composition analysis.

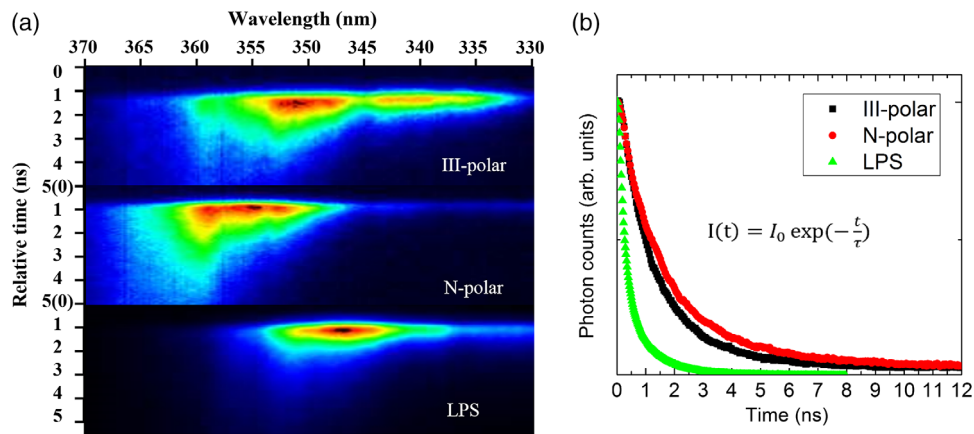


Figure 4. a) Temporal and wavelength-dependent PL spectroscopic profiles at 5 K of uniform III-polar, N-polar and LPS-based MQWs, and b) monoexponential decay curves at peak wavelengths for all three samples.

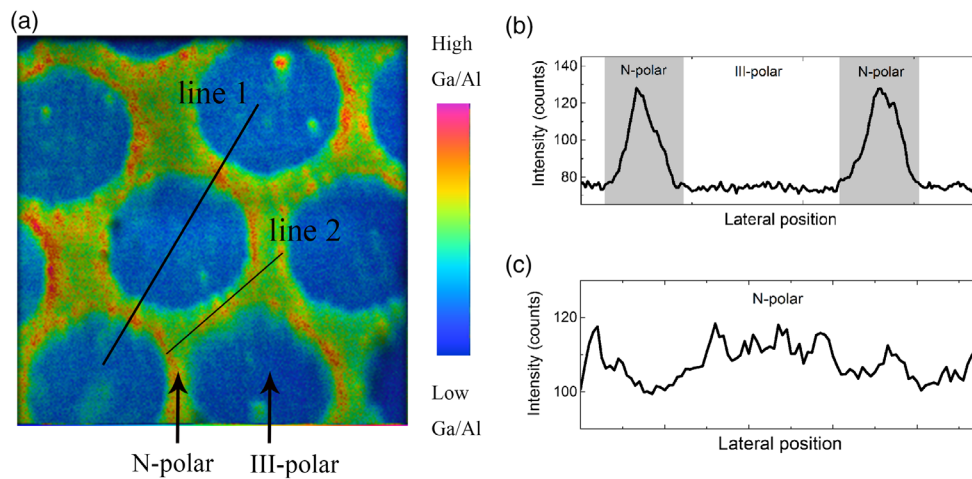


Figure 5. a) Nano-SIMS imaging of the Ga/Al ratios on the surface of the LPS. Red/yellow colors represent larger Ga incorporation, whereas blue color represents smaller Ga incorporation. b,c) Line scans 1# and 2# of the intensity ratios as marked in the color map.

locations are taken to qualitatively analyze the Ga/Al ratio. As marked by the solid line, line 1 scans across several domains, whereas line 2 presents the relative Ga/Al composition within the N-polar domain, and the results are shown in Figure 5b,c, respectively. A higher Ga concentration is revealed in the N-polar than that of the III-polar domains, and the intensity difference reaches 38%. It is well known that Al has smaller diffusion length than Ga atoms;^[32] thus, the lateral transportation in AlGa_N is mainly contributed by Ga. In addition, the lateral diffusion of Ga atoms across the domain boundaries is not uniform due to different surface energies of III- and N-polar domains. Therefore, the large composition difference in adjacent polarity domains is originated from the net mass transport of Ga atoms from III-polar to N-polar domains. This result is consistent with the height difference between two domains in bulk AlGa_N LPS as previously reported by Hoffmann et al.^[33] Within the N-polar domains, the distribution of Ga and Al is also not uniform. Quantum-dot-like features are observed, which are probably caused by the local Ga enrichment. The average intensity

variation is 17%. It must be noted that the MQW consists of AlGa_N QB and Ga_N QW. Therefore, higher Ga/Al ratio in N-polar domains revealed by nano-SIMS means either a higher Ga content in AlGa_N QB or a relatively thicker Ga_N QW (or thinner AlGa_N QB) in the N-polar domains. Both factors can contribute to the carrier localization effect.^[9] In fact, thickness fluctuations in N-polar domain were observed in our previous work, in which case QW/QB nonuniformity was identified in N-polar domain by cross-sectional TEM, whereas sharp interface and uniform QW/QB thickness were obtained in III-polar domain.^[26] This would lead to potential minima in the band structures with a strong carrier localization effect. As a result, luminescence intensity can be greatly enhanced.

Considering that N-polar domains in the LPS have higher Ga content than adjacent III-polar domains if the MQW region is treated as a whole, one would assume that the luminescence peak position of the LPS MQW would be located between those of uniform III- and N-polar samples, because it is a combination of high-Ga-content N-polar domain and low-Ga-content III-polar

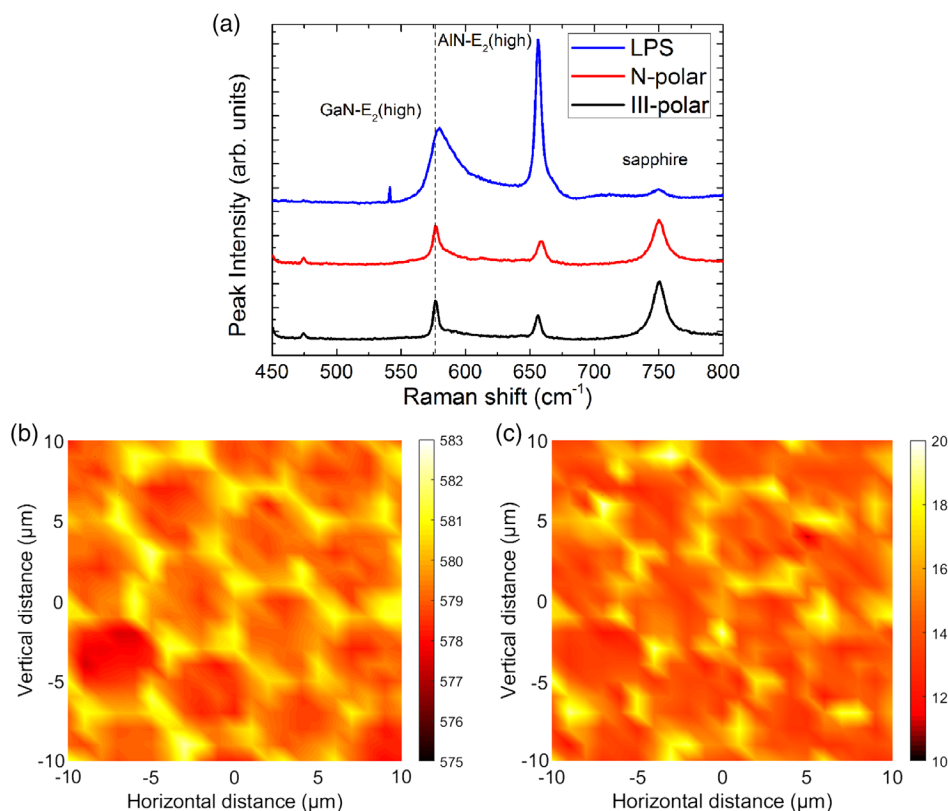


Figure 6. a) Large-scale Raman spectra of uniform III-polar, N-polar, and LPS samples. b,c) Spatially resolved maps of the Raman shift positions (b) and FWHM distributions (c) of the GaN- E_2 (high) mode of LPS.

domain. To the contrary, the PL position of LPS sample is the shortest compared with those of the uniform III- and N-polar ones, as shown in Figure 2a and 4a. Therefore, peak positions of the PL spectra are not exclusively influenced by the average MQW composition, but also by other factors such as strain conditions.^[34] To demonstrate that, **Figure 6a** shows the large-scale Raman spectroscopy of the uniform III-polar, N-polar, and LPS samples. The modes of Al_2O_3 - E_g , GaN- E_2 (high), and AlN- E_2 (high) are clearly observed in the spectra. Compared with the uniform III-polar and N-polar samples, the position of the GaN- E_2 (high) Raman peak shifts right by $\approx 4 \text{ cm}^{-1}$. Note that larger GaN- E_2 (high) Raman shifts are usually associated with increased compressive strains or increased Al composition in AlGaIn.^[35,36] The latter disputes earlier findings of lower Al content (i.e., higher Ga/Al ratio) in N-polar domains demonstrated by nano-SIMSs. Therefore, stronger compressive strains in the N-polar than in III-polar domains must be responsible for the observed Raman peak variation.^[37,38] A conclusion can be safely drawn that the blueshift in PL spectra of LPS is mainly correlated with the strong compressive strains inside the LPS structure. A spatially resolved micro-Raman distribution of GaN- E_2 (high) mode positions is shown in Figure 6b. N-polar domains exhibit larger GaN- E_2 (high) Raman shift compared with III-polar domains. Similarly, N-polar domain has stronger compressive strain than that of III-polar domain. The stronger compressive strains in the N-polar domains can be explained by either higher Ga content and, thus, larger lattice constant of N-polar thin film

in average, or crystal coalescence due to the 3D growth nature of N-polar AlGaIn thin films.

Finally, it needs to be pointed out that the FWHM of the E_2 (high) mode is an indicator for the crystalline quality of epitaxial thin film.^[17] As shown in Figure 6c, the FWHM values of GaN- E_2 (high) mode in N-polar domains are larger than those in III-polar domains by $\approx 5 \text{ nm}$. This can be explained by the existence of high density of grain boundaries and point defects, because N-polar surface is easier to incorporate impurities such as oxygen.^[39] Interestingly, poor crystalline quality does not necessarily result in a poor optical behavior. Carrier localization and enhanced compressive strains compensate the disadvantage of crystalline quality and contribute to the superior optical properties of the LPS-MQW.^[40]

4. Conclusion

AlGaIn/GaN-based UV MQWs with opposite polarity domains were successfully fabricated on a single sapphire substrate. III- and N-polar domains were confirmed by PFM. Stronger PL intensity, shorter wavelength, and higher radiative recombination rate were illustrated for LPS-MQW. The superior optical property of the LPS MQW was ascribed to the carrier localization effect as demonstrated by a thorough investigation on spatially resolved PL mapping, Ga/Al distribution, and strain distribution. This work provides direct evidence of the carrier localization

effect by numerous nanoscale imaging techniques and suggests that the LPS-based MQW is beyond simple combination of III- and N-polar surfaces, offering novel perspective in the realization of high-efficiency UV emitters.

Acknowledgements

This work was supported by the National Key Research and Development Program of China (2016YFB0400802), the National Natural Science Foundation of China (61974149), the Key Research and Development Program of Zhejiang Province (2020C01145), and the Zhejiang Provincial Natural Science Foundation of China (LQ21F040004).

Conflict of Interest

The authors declare no conflict of interest.

Data Availability Statement

Research data are not shared.

Keywords

carrier localization, nanoscale imaging, polarity control, UV emitters

Received: January 17, 2021

Revised: February 19, 2021

Published online:

- [1] S.-I. Inoue, T. Naoki, T. Kinoshita, T. Obata, H. Yanagi, *Appl. Phys. Lett.* **2015**, *106*, 131104.
- [2] W. Guo, Z. Yang, J. Li, X. Yang, Y. Zhang, J. Wang, K. W. Chee, P. Gao, J. Ye, *Nanoscale* **2017**, *9*, 15477.
- [3] M. Kneissl, T.-Y. Seong, J. Han, H. Amano, *Nat. Photonics* **2019**, *13*, 233.
- [4] H. Hu, B. Tang, H. Wan, H. Sun, S. Zhou, J. Dai, C. Chen, S. Liu, L. J. Guo, *Nano Energy* **2020**, *69*, 104427.
- [5] H. Hu, S. Zhou, X. Liu, Y. Gao, C. Gui, S. Liu, *Sci. Rep.* **2017**, *7*, 44627.
- [6] S. Zhou, X. Liu, H. Yan, Z. Chen, Y. Liu, S. Liu, *Opt. Express* **2019**, *27*, A669.
- [7] K. Okamoto, I. Niki, A. Shvarts, Y. Narukawa, T. Mukai, A. Scherer, *Nat. Mater.* **2004**, *3*, 601.
- [8] T. Takano, T. Mino, J. Sakai, N. Noguchi, K. Tsubaki, H. Hirayama, *Appl. Phys. Express* **2017**, *10*, 031002.
- [9] S. Keller, H. Li, M. Laurent, Y. Hu, N. Pfaff, J. Lu, D. F. Brown, N. A. Fichtenbaum, J. S. Speck, S. P. DenBaars, *Semicond. Sci. Technol.* **2014**, *29*, 113001.
- [10] F. Akyol, D. N. Nath, S. Krishnamoorthy, P. S. Park, S. Rajan, *Appl. Phys. Lett.* **2012**, *100*, 231101.
- [11] F. Akyol, D. N. Nath, E. Gür, P. S. Park, S. Rajan, *Jpn. J. Appl. Phys.* **2011**, *50*, 052101.
- [12] S. Keller, N. Fichtenbaum, M. Furukawa, J. Speck, S. DenBaars, U. Mishra, *Appl. Phys. Lett.* **2007**, *90*, 191908.
- [13] S. Mita, *Ph.D. Dissertation*, North Carolina State University, Raleigh, NC, USA, **2008**.
- [14] J. Hite, *J. Cryst. Growth* **2016**, *456*, 133.
- [15] R. N. Collazo, S. Mita, J. Xie, A. Rice, J. Tweedie, R. Dalmau, Z. Sitar, *Phys. Status Solidi A* **2010**, *207*, 45.
- [16] M. Sheikhi, J. Li, F. Meng, H. Li, S. Guo, L. Liang, H. Cao, P. Gao, J. Ye, W. Guo, *IEEE Trans. Electron Devices* **2017**, *64*, 4424.
- [17] R. Kirste, R. Collazo, G. Callsen, M. R. Wagner, T. Kure, J. Sebastian Reparaz, S. Mita, J. Xie, A. Rice, J. Tweedie, *J. Appl. Phys.* **2011**, *110*, 093503.
- [18] R. Collazo, S. Mita, A. Rice, R. F. Dalmau, *Appl. Phys. Lett.* **2007**, *91*, 212103.
- [19] W. Guo, H. Sun, B. Torre, J. Li, M. Sheikhi, J. Jiang, H. Li, S. Guo, K. H. Li, R. Lin, *Adv. Funct. Mater.* **2018**, *28*, 1802395.
- [20] W. Guo, S. Mitra, H. Xu, M. Sheikhi, H. Sun, K. Tian, Zhang, Z.-H., H. Jiang, I. S. Roqan, X. Li, *Optica* **2019**, *6*, 1058.
- [21] H. Xu, J. A. Jiang, Y. Dai, M. Cui, K. H. Li, X. Ge, J. Hoo, L. Yan, S. Guo, J. Ning, *ACS Appl. Nano Mater.* **2020**, *3*, 5335.
- [22] P. Gao, J. He, S. Zhou, X. Yang, S. Li, J. Sheng, D. Wang, T. Yu, J. Ye, Y. Cui, *Nano Lett.* **2015**, *15*, 4591.
- [23] P. Dong, J. Yan, Y. Zhang, J. Wang, J. Zeng, C. Geng, P. Cong, L. Sun, T. Wei, L. Zhao, *J. Cryst. Growth* **2014**, *395*, 9.
- [24] M. D. Brubaker, S. M. Duff, T. E. Harvey, P. T. Blanchard, A. Roshko, A. W. Sanders, N. A. Sanford, K. A. Bertness, *Cryst. Growth Des.* **2015**, *16*, 596.
- [25] T. Narita, Y. Honda, M. Yamaguchi, N. Sawaki, *Phys. Status Solidi B* **2006**, *243*, 1665.
- [26] W. Guo, H. Sun, B. Torre, J. Li, M. Sheikhi, J. Jiang, H. Li, S. Guo, K. H. Li, R. Lin, *Adv. Funct. Mater.* **2018**, *28*, 1802395.
- [27] W. Guo, S. Mitra, J. A. Jiang, H. Xu, J. Ye, *Optica* **2019**, *6*, 1058.
- [28] N. Alfaraj, S. Mitra, F. Wu, I. A. Ajia, B. Janjua, A. Prabaswara, R. A. Aljefri, H. Sun, T. Khee Ng, B. S. Ooi, *Appl. Phys. Lett.* **2017**, *110*, 011105.
- [29] I. A. Ajia, Y. Yamashita, K. Lorenz, M. Muhammed, L. Spasevski, D. Almalawi, J. Xu, K. Iizuka, Y. Morishima, D. H. Anjum, *Appl. Phys. Lett.* **2018**, *113*, 082102.
- [30] Z. Bryan, I. Bryan, S. Mita, J. Tweedie, Z. Sitar, R. Collazo, *Appl. Phys. Lett.* **2015**, *106*, 232101.
- [31] S. Schlichting, G. M. O. Höning, J. Müßener, P. Hille, T. Grieb, S. Westerkamp, J. Teubert, J. Schörmann, M. R. Wagner, R. Rosenauer, M. Eickhoff, A. Hoffmann, G. Callsen *Commun. Phys.* **2018**, *1*, 48.
- [32] T. Narita, T. Hikosaka, Y. Honda, M. Yamaguchi, N. Sawaki, *Phys. Status Solidi C* **2003**, *7*, 2154.
- [33] M. P. Hoffmann, R. Kirste, S. Mita, W. Guo, J. Tweedie, M. Bobea, I. Bryan, Z. Bryan, M. Gerhold, R. Collazo, *Phys. Status Solidi A* **2015**, *212*, 1039.
- [34] Z. Bryan, I. Bryan, S. Mita, J. Tweedie, Z. Sitar, R. Collazo, *Appl. Phys. Lett.* **2015**, *106*, 4323.
- [35] J. Kim, A. Kimura, Y. Kamei, N. Hasuike, H. Harima, K. Kisoda, Y. Simahara, H. Miyake, K. Hiramatsu, *J. Appl. Phys.* **2011**, *110*, 033511.
- [36] C. Kisielowski, J. Krüger, S. Ruvimov, T. Suski, J. Ager III, E. Jones, Z. Liliental-Weber, M. Rubin, E. Weber, M. Bremser, *Phys. Rev. B* **1996**, *54*, 17745.
- [37] R. Kirste, S. Mita, L. Hussey, M. P. Hoffmann, W. Guo, I. Bryan, Z. Bryan, J. Tweedie, J. Xie, M. Gerhold, *Appl. Phys. Lett.* **2013**, *102*, 181913.
- [38] W. Tian, W. Y. Yan, X. Hui, S. L. Li, Y. Y. Ding, Y. Li, Y. Tian, J. N. Dai, Y. Y. Fang, Z. H. Wu, *J. Appl. Phys.* **2012**, *112*, 252.
- [39] S. Keller, H. Li, M. Laurent, Y. Hu, N. Pfaff, J. Lu, D. F. Brown, N. A. Fichtenbaum, J. S. Speck, S. P. DenBaars, U. K. Mishra, *Semicond. Sci. Technol.* **2014**, *29*, 113001.
- [40] P. J. Schuck, M. D. Mason, R. D. Grober, O. Ambacher, A. P. Lima, C. Miskys, R. Dimitrov, M. Stutzmann, *Appl. Phys. Lett.* **2001**, *79*, 952.